Patch Ordering-Based SAR Image Despeckling Via Transform-Domain Filtering

Bin Xu, Yi Cui, *Member, IEEE*, Zenghui Li, Bin Zuo, Jian Yang, *Senior Member, IEEE*, and Jianshe Song

***Abstract*—In this paper, we propose a synthetic aperture radar (SAR) image despeckling method based on patch ordering and transform-domain filtering. Logarithmic transformation with bias correction is applied to the original SAR image to transform the multiplicative noise model into the additive model. Then, we adopt a two-stage filtering strategy. The first stage is coarse filtering which can suppress speckle effectively. In this stage, we extract the sliding patches from the logarithmic SAR image, and order them in a smooth way by a simplified patch ordering algorithm specially for SAR images. The ordered patches are filtered by learned simultaneous sparse coding (SSC), a technology recently advanced in image processing. Then, the coarse filtering result is reconstructed from the filtered patches via inverse permutation and subimage averaging. The second stage is refined filtering which can eliminate small artifacts generated by the coarse filtering. In this stage, the sliding patches are extracted from the coarse filtering result and ordered in the same way. Then, we apply 2-D wavelet hard-thresholding to the ordered patches and reconstruct the refined filtering result. The final result is obtained by taking exponential transformation to the refined filtering result. An algorithm based on the proposed strategy is presented in detail and the parameters are selected for fast and effective realization. Experimental results with both simulated images and real SAR images demonstrate that the proposed method achieves state-of-the-art despeckling performance in terms of peak signal-to-noise ratio (PSNR), structural similarity (SSIM) index, equivalent number of looks (ENLs), and ratio image.**

***Index Terms*—Despeckling, patch ordering, simultaneous sparse coding (SSC), synthetic aperture radar (SAR).**

I. Introduction

SYNTHETIC aperture radar (SAR) images, being acquired via coherent imaging, are intrinsically associated with a noise-like phenomenon called speckle. The presence of speckle affects the performance in many applications of SAR image processing. For example, it increases the false alarm rate in target/edge detection [1] and decreases the correct classification rate in terrain classification [2]. Thus, SAR image despeckling is an important preprocessing step and many methods have been proposed during the past three decades. In general, the speckle in SAR images is characterized by the multiplicative noise model [3]. The purpose of despeckling is to recover the underlying target backscattering coefficient from the observed intensity image.

To make this problem easier, the multiplicative model can be transformed into the additive model via homomorphic transformation [4] by taking the logarithm of the noisy image. Then, the image denoising methods developed for the additive noise case can be applied to the logarithmic SAR image, such as wavelet shrinkage [5], [6], total variation [7], sparse representation [8], [9], and so on. Another commonly used approach is to write the multiplicative noise in an additive but signal-dependent way [14]. Many classical despeckling techniques adopt this model and perform filtering in the spatial domain based on the minimum mean square error (MMSE) criterion [14]–[17] or the maximum *a posteriori* (MAP) criterion [18], [19]. Some advanced methods also adopt the additive signal-dependent model, but operate in the wavelet domain [20]–[23] or nonsubsampled shearlet transform domain [24].

In addition, the nonlocal means (NLM) algorithm proposed by Buades *et al.* [25] provides a breakthrough in image denoising. This approach utilizes the similarity between the patches surrounding the estimated and the selected pixels to obtain the weight for pixel averaging in a large region. The NLM algorithm has also been extended to SAR [26]–[28] and polarimetric SAR [29] image despeckling. In particular, the probabilistic patch-based (PPB) algorithm [27] replaces the Euclidean distance in [25] by a statistical similarity criterion based on the Nakagami–Rayleigh distribution and achieves very good results in SAR image despeckling. Inspired by the block matching 3-D (BM3D) algorithm [30], Parrilli *et al.* [23] proposed a SAR version of BM3D, i.e., SAR-BM3D, using local linear MMSE criterion and undecimated wavelet. Later, Cozzolino *et al.* [31] proposed a fast adaptive nonlocal SAR (FANS) despeckling method based on SAR-BM3D. On the other hand, image denoising via sparse representation has also attracted an increasing amount of attention [34]–[36]. Elad and Aharon [34] proposed an image denoising method based on sparse representations over learned dictionaries which can be acquired by the K-SVD algorithm [37]. Mairal *et al.* [36] proposed the nonlocal sparse model for image denoising by combining the nonlocal method and simultaneous sparse coding (SSC). Most recently, the sparse model has been successfully applied to SAR image despeckling and found to be promising for multiplicative noise removal [8]–[12].

Manuscript received January 18, 2014; revised November 08, 2014; accepted November 18, 2014. Date of publication December 17, 2014; date of current version May 26, 2015. This work was supported in part by the NSFC under Grant 41171317, in part by the key project of the NSFC under Grant 61132008, in part by the major research plan of the NSFC under Grant 61490693, and in part by the Research Foundation of Tsinghua University.

B. Xu, Z. Li, B. Zuo, and J. Yang are with the Department of Electronic Engineering, Tsinghua University, Beijing 100084, China (e-mail: xubin07161@gmail.com; sunshinenudt@gmail.com; zuob2009@126.com; yangjian_ee@mail.tsinghua.edu.cn).

Y. Cui is with the Global Institute for Collaborative Research and Education, Hokkaido University, Sapporo 060-0808, Japan (e-mail: cuiyi.trea@gmail.com).

J. Song is with Xi'an Research Institute of Hi-Technology, Xi'an 710025, China (e-mail: Songjianshe09@126.com).

Color versions of one or more of the figures in this paper are available online at http://ieeexplore.ieee.org.

Digital Object Identifier 10.1109/JSTARS.2014.2375359

In this paper, we also propose to address SAR despeckling in the transformed image domain via sparse representation. Similarly, we work on the logarithmic SAR images because of the reported better performance for the log-intensity data [8]. However, our method is different from previous works in the following two aspects. First, we apply transform-domain filtering to the ordered SAR patches rather than the original image. In particular, inspired by the work of Ram *et al.* [32], [33], we have designed a SAR-oriented patch ordering algorithm by the similarity measure based on SAR statistics. This procedure can effectively improve the signal regularity and hence enhance the performance of sparse representation. Second, we propose a two-stage strategy to both deal with speckle reduction and artifact elimination. Specifically, in the first stage (coarse filtering), the main purpose is to effectively remove the noise. Therefore, we filter the ordered patches with SSC because of their superior noise reduction ability combined. Then in the second stage, we apply patch ordering to the coarse filtering result again and process the ordered patches by 2-D wavelet for refined filtering. Finally, the despeckled image is reconstructed from the refined result by inverse permutation and subimage averaging.

It is worth mentioning that our motivation to propose the aforementioned two-stage algorithm in fact stems from the well-known observation that any single-stage transform-domain is susceptible to produce artifacts. This phenomenon is especially significant when the signal-to-noise ratio (SNR) becomes worse as that in SAR imagery. The solution proposed here is then to exploit different transformation bases, which is based on the intuitive idea that independent transform-domain filtering methods will often produce complementary artifacts. For example, it is very likely that the learned dictionary by K-SVD and the wavelet basis, one being image dependent and one generic, are responsible for spurious artifacts at different places. Since most of these artifacts appear like high-frequency noisy components, applying the second stage of filtering will effectively remove those artifacts associated with the first stage. Importantly, although the second stage of filtering may still produce new artifacts (ringing effects if using wavelets), it is important to notice that the sole purpose at the second stage is to remove a small number of isolated artifacts rather than the ubiquitous noise (task already accomplished by the first stage). Thus, we are actually allowed to use a rather conservative value for thresholding wavelet coefficients, which can efficiently suppress the artifacts from the first stage and at the same time avoid secondary ones that might ensue. This will be verified both visually and numerically in Section V.

The rest of the paper is organized as follows. Section II presents the logarithmic SAR image statistics and patch ordering. Section III describes the proposed algorithm in detail. Section IV gives the efficient realization of the proposed method. Section V reports the experimental results. Finally, Section VI concludes this paper.

II. Logarithmic SAR Image Statistics and Patch Ordering

In this section, we introduce two important preprocessing steps that will be used throughout this paper. Since we perform filtering on the log-intensity data, we first review the logarithmic SAR statistics from which we can obtain the mean and variance of the log-transformed speckle. This information will be fed to our algorithm for bias removal and setting of filtering parameters. Second, we describe the image filtering framework of patch ordering that precedes each step of transform-domain filtering. Particularly, we propose a new patch ordering algorithm that adapts to the nature of SAR data and furthermore take two simplifying measures in order to reduce the computation complexity.

A. Logarithmic SAR Image Statistics

In SAR images, the speckle is characterized by the multiplicative noise model [3]

$$I = xv \tag{1}$$

where I is the observed intensity (noisy image); x is the underlying target backscattering coefficient (noise-free image); and v is the speckle (multiplicative noise). It is well established that fully developed speckle follows the Gamma distribution [3]

$$p_v(v) = \frac{L^L v^{L-1}}{\Gamma(L)} \exp(-vL), \quad v \geq 0 \tag{2}$$

where L is the equivalent number of looks (ENLs) and $\Gamma()$ is the Gamma function. The ENL can be effectively obtained by supervised [3] or unsupervised estimation [38], [39]. For a homogeneous region, the ENL can be calculated by

$$L = \frac{(\text{mean})^2}{\text{var}}. \tag{3}$$

Thus, the ENL is treated as a known parameter in this paper.

By logarithmic transformation of (1), the multiplicative noise becomes additive, i.e.,

$$\ln(I) = \ln(x) + \ln(v). \tag{4}$$

The mean and variance of $\ln(v)$ are related to the ENL [13] by

$$E[\ln(v)] = \psi^{(0)}(L) - \ln(L) \tag{5}$$

$$\text{var}[\ln(v)] = \psi^{(1)}(L) \tag{6}$$

where $\psi^{(m)}(L)$ is the polygamma function of order m.

Then the log-intensity SAR image with bias correction is

$$I^{(\ln)} = \ln(I) - \psi^{(0)}(L) + \ln(L). \tag{7}$$

The following filtering process will work on the bias-corrected log-intensity data, $I^{(\ln)}$.

B. Image Filtering Framework of Patch Ordering

The original image filtering framework of patch ordering is shown in Fig. 1 [32], [33]. In general, the sliding patches extracted from the input image are first ordered and permuted. Then, these ordered patches are filtered (in the work

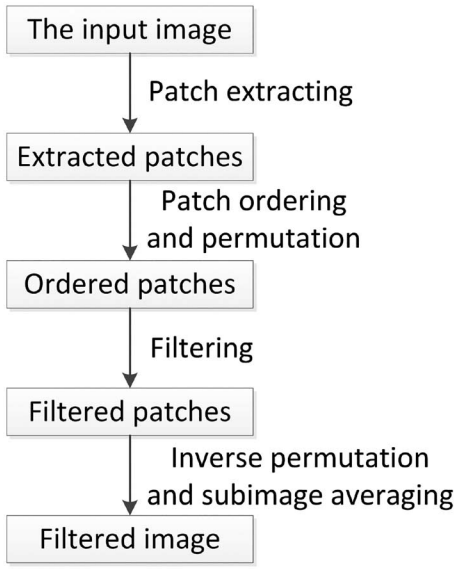

Fig. 1. Image filtering framework of patch ordering.

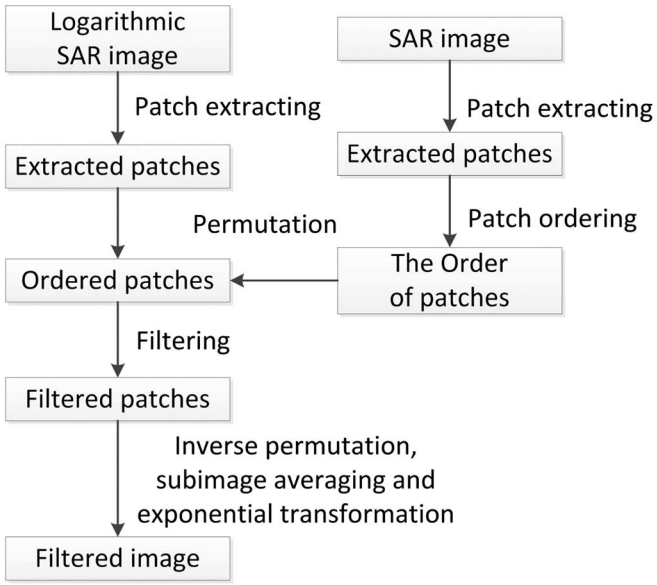

Fig. 2. Image filtering framework used in this study.

of Ram *et al.* [32], [33], spatial filtering is applied). The final result can be reconstructed from the filtered patches via inverse permutation and subimage averaging.

Specifically for filtering SAR images, the patch ordering framework needs to be adapted as shown in Fig. 2. Because we are working on the log-intensity data, the patches are extracted from the logarithmically transformed SAR image. Nevertheless, ordering and permutation of these patches will still be implemented based on their similarity from the original (amplitude) SAR image as will be proposed in Section II-C. Details of the filtering methods for the ordered patches will be described in Section III.

Algorithm 1. Simplified patch ordering algorithm for SAR images

Input: The image patches $\mathbf{y}_i(i = 1, \ldots, N^{(p)})$.
Parameter: The search range $C \times C$.
Choose the first patch as the initial patch, i.e. $\Omega(1) = 1$.
for $i = 1$ to $N^{(p)} - 1$ **do**
Let $\mathbf{y}_{\Omega(i)}$ and Q_i be the current patch and the set of indices of the search range around $\mathbf{y}_{\Omega(i)}$, respectively.
if $|Q_i \backslash \Omega| \geq 1$[1], **then**
Calculate the BSM of $\mathbf{y}_l$ and $\mathbf{y}_{\Omega(i)}$ by (9), where $l \in Q_i \backslash \Omega$. Choose the patch $\mathbf{y}_{\hat{l}}$ corresponding to the smallest BSM.
else
Choose the spatially nearest patch $\mathbf{y}_{\hat{l}}$ to $\mathbf{y}_l$, where $\hat{l} \notin \Omega$.
end if
$\Omega(i+1) = \hat{l}$
end for
Output: The set Ω which holds the ordering.

C. Patch Ordering for SAR Images

Suppose that the size of I is $N_1 \times N_2$. We extract the sliding patches of size $\sqrt{n} \times \sqrt{n}$ from I. If the sliding step is $SL^{(p)}$, then the number of patches is

$$N^{(p)} = \left(\left\lceil \frac{N_1 - \sqrt{n}}{SL^{(p)}} \right\rceil + 1 \right) \left(\left\lceil \frac{N_2 - \sqrt{n}}{SL^{(p)}} \right\rceil + 1 \right) \quad (8)$$

where $\lceil \cdot \rceil$ is the ceil function.

Let $\mathbf{y}_i(i = 1, \ldots, N^{(p)})$ be the column stacked version of these patches. The purpose of patch ordering is to reorder these patches in a smooth way. The original patch ordering algorithm [32] utilizes the Euclidean distance as the similarity measurement. In addition, it has randomness in order to facilitate the cycle-spinning method [40]. However, the Euclidean distance is not an appropriate choice for SAR images. Here we employ the block similarity measure (BSM) [23], [27] as the similarity measurement. The BSM of $\mathbf{y}_i$ and $\mathbf{y}_l$ is

$$BSM_{i,l} = \sum_j \ln \left[\frac{\sqrt{\mathbf{y}_i(j)}}{\sqrt{\mathbf{y}_l(j)}} + \frac{\sqrt{\mathbf{y}_l(j)}}{\sqrt{\mathbf{y}_i(j)}} \right]. \quad (9)$$

We further take the following two measures to reduce the computation complexity of patch ordering. First, we drop the cycle-spinning method due to its high computational cost in exchange of only small performance improvement. Second, as suggested in [32], we also restrict the search range to a $C \times C$ neighborhood surrounding the current patch. The detail of the simplified patch ordering algorithm for SAR images is shown in Algorithm 1.

Suppose that $\mathbf{Y}$ and $\mathbf{Z}$ are the patches before and after patch ordering, respectively,

$$\mathbf{Y} = [\mathbf{y}_1 \cdots \mathbf{y}_{N^{(p)}}] \quad (10)$$

$$\mathbf{Z} = [\mathbf{z}_1 \cdots \mathbf{z}_{N^{(p)}}]. \quad (11)$$

[1]Here, $|\cdot|$ is the number of elements within a set and "\" is the set difference.

Then we have

$$\mathbf{Z} = \mathbf{Y}\mathbf{P}_{\Omega} \tag{12}$$

where $\mathbf{P}_{\Omega}$ is the $N^{(p)} \times N^{(p)}$ permutation matrix corresponding to the set Ω which holds the ordering.

III. Algorithm

In this paper, we propose a new SAR image despeckling algorithm based on the image filtering framework shown in Fig. 2. Instead of applying spatial filtering [32], [33] to the ordered patches, we propose to use transform domain methods, i.e., sparse representation [34] and wavelet [30], [45] to fulfill this purpose. Moreover, the proposed algorithm consists of two stages. In the first stage, the log-intensity SAR image is filtered by patch ordering and SSC. Although denoising via SSC can suppress speckle effectively, it produces small artifacts (see the results in Section V) which are caused by the learned dictionary [43]. Thus the first stage is a coarse filtering stage. The artifacts generated by sparse representation can be alleviated by other transform domain methods. To handle this, we adopt a refined filtering stage in which the coarse filtering result is filtered by patch ordering and 2-D wavelet hard-thresholding. The complete procedure is hierarchically illustrated in Fig. 3 and summarized in Algorithm 2.

A. Step 1: Coarse Filtering Via SSC

When the ENL is small, the SNR of a logarithmic SAR image is relatively low. In order to improve the accuracy of patch ordering, a 3×3 Boxcar filter is first applied to I and the subsequent patch ordering works on the Boxcar filtering result I_B. Let $\mathbf{Y}_1$ and $\mathbf{Y}_B$ be the patches extracted from $I^{(\ln)}$ and I_B, respectively. We can get set Ω_1 from $\mathbf{Y}_B$ by Algorithm 1. Then the ordered patches $\mathbf{Z}_1$ can be obtained by

$$\mathbf{Z}_1 = \mathbf{Y}_1 P_{\Omega_1}. \tag{13}$$

In the coarse filtering stage, the ordered patches are filtered by simultaneous sparse representation. The core idea of sparse representation [34] is that the clean signal can be represented by a linear combination of few atoms in a redundant dictionary. Then denoising a patch $\mathbf{z}_i \in \mathbb{R}^n$ aims to solve

$$\min_{\boldsymbol{\alpha}_i} \|\boldsymbol{\alpha}_i\|_0 \ \text{ s.t. } \ \|\mathbf{z}_i - \mathbf{D}\boldsymbol{\alpha}_i\|_2^2 \le \varepsilon \tag{14}$$

where $\mathbf{D} \in \mathbb{R}^{n \times k} (k > n)$ is an overcomplete dictionary; $\boldsymbol{\alpha}_i \in \mathbb{R}^k$ is the sparse representation of $\mathbf{z}_i$; and ε is related to the noise variance. It should be noted that the ℓ_2-norm used in (14) is not the optimal choice for the logarithmic speckle. However, as shown in Fig. 4, the noise in logarithmic SAR images tends to become Gaussian with the increase in the ENL [23]. Thus, it is reasonable to adopt the ℓ_2-norm in (14).

Algorithm 2. The proposed algorithm for SAR image despeckling

Input: The input SAR image I, the ENL L.

Step 1: Coarse filtering.

Boxcar filtering. Apply a 3×3 Boxcar filter to I, and obtain the filtering result I_B.

Logarithmic transformation with bias correction. Calculate the log-intensity image $I^{(\ln)}$ by taking the logarithmic transformation with bias correction to I.

Patch extracting. Extract the sliding patches $\mathbf{Y}_B$ and $\mathbf{Y}_1$ of size $\sqrt{n_1} \times \sqrt{n_1}$ from I_B and $I^{(\ln)}$, respectively.

Patch ordering. Order the patches $\mathbf{Y}_B$ by Algorithm 1, and obtain the set Ω_1. Then calculate the ordered patches $\mathbf{Z}_1$ by $\mathbf{Z}_1 = \mathbf{Y}_1 P_{\Omega_1}$.

Denoising via SSC. Denoise $\mathbf{Z}_1$ by Algorithm 3, and obtain the filtering result $\hat{\mathbf{Z}}_1$. Then perform inverse permutation on $\hat{\mathbf{Z}}_1$, i.e. $\hat{\mathbf{Y}}_1 = \hat{\mathbf{Z}}_1 P_{\Omega_1}^{-1}$.

Subimage averaging. Reconstruct the filtering result $\hat{I}_1^{(\ln)}$ from $\hat{\mathbf{Y}}_1$ by subimage averaging [32].

Exponential transformation. Calculate the coarse filtering result $\hat{x}_1$ by applying exponential transformation to $\hat{I}_1^{(\ln)}$.

Step 2: Refined filtering.

Patch extracting. Extract the sliding patches $\mathbf{Y}^{(\mathrm{C})}$ and $\mathbf{Y}_2$ of size $\sqrt{n_2} \times \sqrt{n_2}$ from $\hat{x}_1$ and $\hat{I}_1^{(\ln)}$, respectively.

Patch ordering. Order the patches $\mathbf{Y}^{(\mathrm{C})}$, and obtain the set Ω_2. Then calculate the ordered patches $\mathbf{Z}_2$ by $\mathbf{Z}_2 = \mathbf{Y}_2 P_{\Omega_2}$.

Denoising via 2-D wavelet hard-thresholding. Denoise $\mathbf{Z}_2$ by 2-D wavelet hard-thresholding, and obtain the filtering result $\hat{\mathbf{Z}}_2$. Then perform inverse permutation on $\hat{\mathbf{Z}}_2$, i.e. $\hat{\mathbf{Y}}_2 = \hat{\mathbf{Z}}_2 P_{\Omega_2}^{-1}$.

Subimage averaging. Reconstruct the filtering result $\hat{I}_2^{(\ln)}$ from $\hat{\mathbf{Y}}_2$ by subimage averaging.

Exponential transformation. Calculate the final filtering result $\hat{x}_2$ by applying exponential transformation to $\hat{I}_2^{(\ln)}$.

Output: The final filtering result $\hat{x}_2$.

Algorithm 3. Denoising Via SSC

Input: The ordered patches $\mathbf{Z}$, the ENL L.

Parameter: The number of patches within a group $N^{(S)}$, the number of groups for dictionary training $N^{(t)}$, the number of training iterations $N^{(i)}$, the size of dictionary $n \times k$.

Dictionary learning stage: Randomly choose $N^{(t)}$ groups for dictionary learning. Use the KSVD algorithm to train the dictionary by replacing the sparse coding stage in [37] with the SSC problem (17).

SSC stage: Perform the denoising on each group via SSC. Compute the final result $\hat{\mathbf{Z}}^{(SSC)}$ by weighted averaging the filtering results of all groups.

Output: The filtering result $\hat{\mathbf{Z}}^{(SSC)}$.

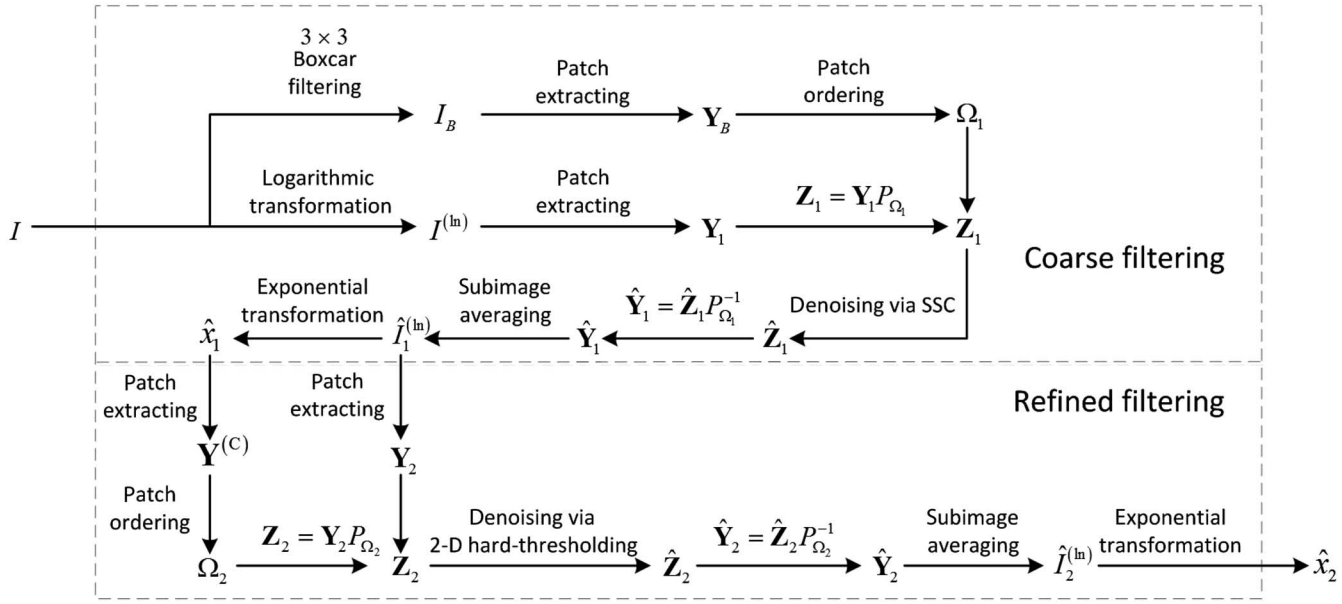

Fig. 3. Flowchart of the proposed algorithm.

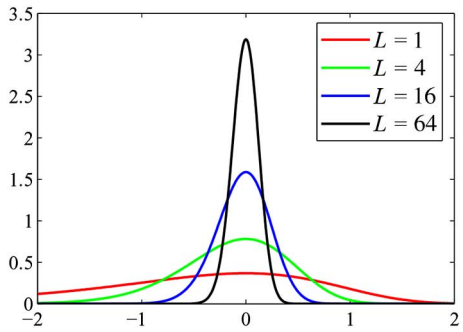

Fig. 4. PDF of the logarithmic speckle where $L = 1$, 4, 16, and 64.

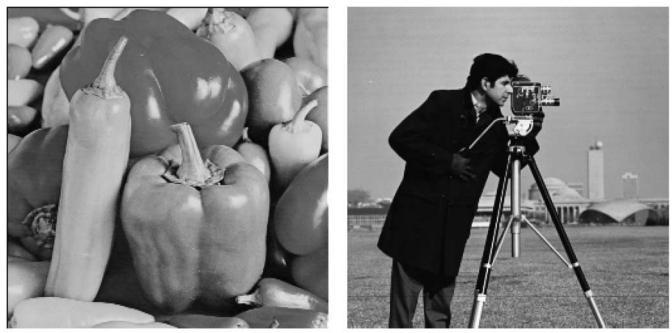

(a) (b)

Fig. 5. Test speckle free images. (a) Peppers. (b) Cameraman.

TABLE I
PARAMETERS USED IN THE PROPOSED ALGORITHM

Coarse filtering	n_1	C	$SL_1^{(p)}$	$N^{(S)}$	$N^{(t)}$	$N^{(i)}$	k
	64	17	2	8	2000	5	512
Refined filtering	n_2	$SL_2^{(p)}$	$\mathcal{T}$		λ		
	36	1	2D-Haar		$0.95\sqrt{\psi^{(1)}(L)}$		

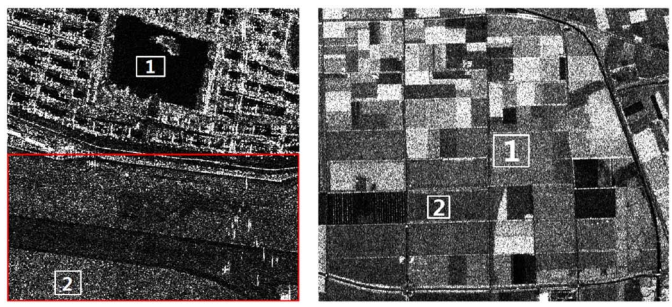

(a) (b)

Fig. 6. Test SAR images. The pixels in the white box are used for ENL estimation. (a) Dalian (600 × 600), $L = 1.00$. The pixels in the red box are used to analyze the ratio image. (b) Flevoland (500 × 600), $L = 2.99$. The whole image is used to analyze the ratio image.

According to (6), for log-intensity SAR images

$$\varepsilon = n\psi^{(1)}(L). \tag{15}$$

The dictionary $\mathbf{D}$ can be trained by the K-SVD algorithm. With the learned dictionary, the sparse decomposition problem (14) can be solved by the OMP algorithm [41]. Then the filtering result of $\mathbf{z}_i$ is

$$\hat{\mathbf{z}}_i = \mathbf{D}\boldsymbol{\alpha}_i. \tag{16}$$

Unlike sparse representation, the core idea of SSC [42] is that several similar signals can be represented by different linear combinations of the same atoms. Then denoising several similar patches $\mathbf{z}_i (i \in S)$ amounts to solving

$$\min_{\boldsymbol{\Lambda}} \|\boldsymbol{\Lambda}\|_{0,\infty} \ \text{s.t.} \ \sum_{i \in S} \|\mathbf{z}_i - \mathbf{D}\boldsymbol{\alpha}_i\|_2^2 \le \varepsilon' \tag{17}$$

TABLE II
PSNR (dB) RESULTS FOR PEPPERS AND CAMERAMAN

	Peppers					Cameraman				
	$L=1$	$L=2$	$L=4$	$L=8$	$L=16$	$L=1$	$L=2$	$L=4$	$L=8$	$L=16$
Noisy	12.01	14.80	17.69	20.67	23.67	12.02	14.79	17.71	20.68	23.67
PPB	23.86	25.50	26.95	28.43	29.86	23.17	24.77	26.21	27.60	28.89
MIDAL	23.63	25.56	27.47	29.02	29.91	23.11	24.66	26.28	28.19	29.48
SAR-BM3D	**24.91**	26.56	28.11	29.72	31.37	**24.99**	26.43	27.95	29.64	31.40
H-PO	24.07	26.42	28.35	30.02	31.64	23.21	25.45	27.16	28.75	30.37
Coarse filtering	23.26	25.72	27.93	29.84	31.62	22.92	25.38	27.37	29.25	31.14
Refined filtering	24.58	**26.93**	**28.87**	**30.67**	**32.33**	24.39	**26.48**	**28.17**	**29.90**	**31.63**

Best results are emphasized in boldface.

TABLE III
SSIM RESULTS FOR PEPPERS AND CAMERAMAN

	Peppers					Cameraman				
	$L=1$	$L=2$	$L=4$	$L=8$	$L=16$	$L=1$	$L=2$	$L=4$	$L=8$	$L=16$
Noisy	0.172	0.244	0.332	0.433	0.543	0.267	0.337	0.409	0.483	0.561
PPB	0.678	0.739	0.790	0.831	0.865	0.662	0.722	0.774	0.819	0.861
MIDAL	0.710	0.774	0.814	0.820	0.846	0.697	0.751	0.787	0.791	0.808
SAR-BM3D	**0.747**	0.798	0.838	0.872	0.897	**0.752**	**0.793**	**0.832**	**0.871**	**0.906**
H-PO	0.698	0.779	0.834	0.863	0.887	0.692	0.752	0.803	0.827	0.852
Coarse filtering	0.626	0.725	0.796	0.849	0.883	0.607	0.710	0.785	0.845	0.889
Refined filtering	0.737	**0.802**	**0.846**	**0.877**	**0.901**	0.735	0.789	0.828	0.864	0.899

Best results are emphasized in boldface.

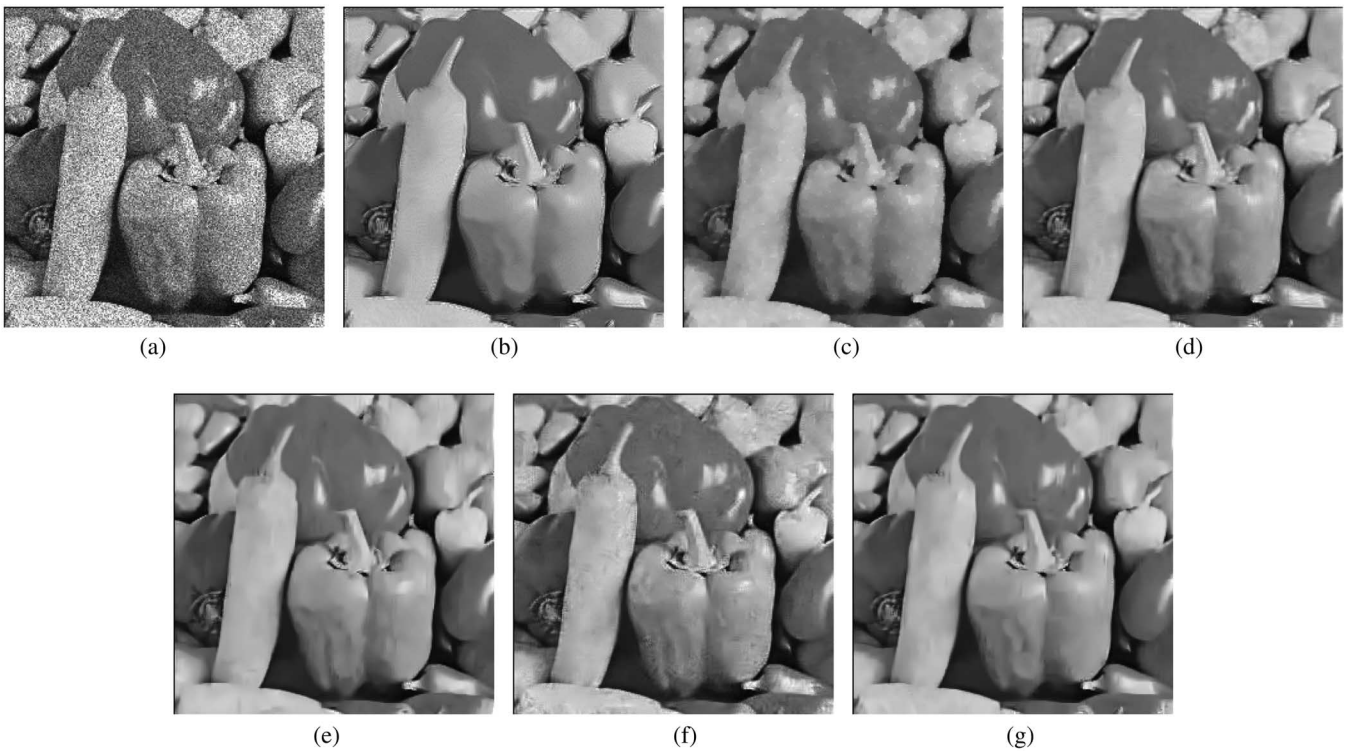

Fig. 7. Filtered images for Peppers contaminated by 4-look speckle. (a) Noisy image. (b) PPB. (c) MIDAL. (d) SAR-BM3D. (e) H-PO. (f) Coarse filtering. (g) Refined filtering.

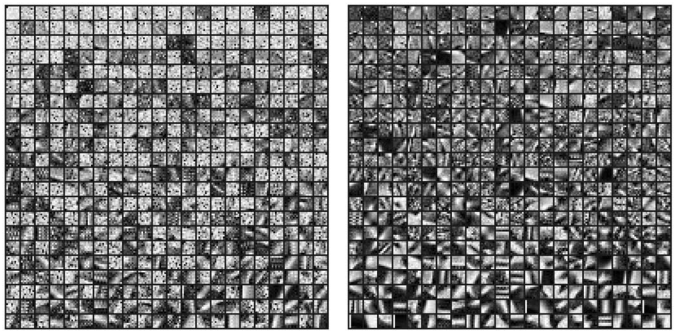

(a) (b)

Fig. 8. Learned dictionaries in the proposed method for Peppers. (a) $L = 1$. (b) $L = 4$.

where S is the set of similar patches, and $\mathbf{\Lambda}$ is

$$\mathbf{\Lambda} = (\cdots \boldsymbol{\alpha}_i \cdots)_{i \in S}. \tag{18}$$

where $\|\mathbf{\Lambda}\|_{0,\infty}$ is a pseudo norm [42] which stands for the number of nonzero rows of $\mathbf{\Lambda}$. For log-intensity SAR images, ε' can be obtained by

$$\varepsilon' = nN^{(S)}\psi^{(1)}(L) \tag{19}$$

where $N^{(S)}$ is the number of elements in set S. In general, the similarity of neighboring patches in $\mathbf{Z}_1$ is relatively high. Thus, we use $N^{(S)}$ neighboring patches to form a group, and then perform SSC on each group.

The K-SVD algorithm can also be adopted to train the dictionary $\mathbf{D}$ by replacing the sparse coding stage in [37] with the SSC problem (17). Then, (17) can be solved by the S-OMP algorithm [42] and $\mathbf{D}\boldsymbol{\alpha}_i$ is the estimate of $\mathbf{z}_i$. The denoising method via SSC is summarized in Algorithm 3.

Let $\hat{\mathbf{Z}}_1$ be the filtered patches obtained by Algorithm 3. Then, the coarse filtering result $\hat{x}_1$ can be reconstructed from $\hat{\mathbf{Z}}_1$ via inverse permutation, subimage averaging, and exponential transformation.

B. Step 2: Refined Filtering Via 2-D Wavelet Hard-Thresholding

The aim of the refined filtering stage is to reduce the artifacts generated in the coarse filtering stage. Different transform-domain filtering methods will produce different kinds of artifacts. The artifacts generated by sparse representation can be alleviated by other transform-domain filtering methods. Here we choose wavelets to accomplish such task.

We apply patch ordering to $\hat{x}_1$ and obtain the set Ω_2. Let $\mathbf{Y}_2$ be the patches extracted from the logarithm of $\hat{x}_1$. Then, the ordered patches $\mathbf{Z}_2$ can be obtained by

$$\mathbf{Z}_2 = \mathbf{Y}_2\mathbf{P}_{\Omega_2}. \tag{20}$$

Denoising the ordered patches $\mathbf{Z}_2$ via 2-D wavelet hard-thresholding can be easily accomplished by

$$\hat{\mathbf{Z}}_2 = \mathcal{T}^{-1}(\Upsilon(\mathcal{T}(\mathbf{Z}_2))) \tag{21}$$

where $\mathcal{T}$ is the 2-D wavelet transform; $\mathcal{T}^{-1}$ is the corresponding inverse transform; Υ is the hard-thresholding operator with threshold λ. It should be noted that wavelet hard-thresholding will introduce new artifacts in the refined filtering stage. However, with suitable threshold, it can alleviate the artifacts in $\hat{x}_1$ effectively and only generate few artifacts.

The final filtering result $\hat{x}_2$ can be reconstructed from $\hat{\mathbf{Z}}_2$ in the same way as described in the coarse filtering stage.

IV. Efficient Realization

In this section, we first discuss the selection of transform-domain filtering methods. Then we present the parameter selection. The parameters suggested to be used in the proposed algorithm are listed in Table I. These parameters have been tested and found effective over a variety of simulated/real SAR images and will be fixed for performance evaluation in Section V.

A. Selection of Transform-Domain Filtering Methods

Considering our primary goal (i.e., despeckling), the first stage of coarse filtering should be able to remove the noise effectively. To the best of our knowledge, simultaneous sparse representation is one of the best image filtering methods and has very strong noise reduction ability. Moreover, neighboring patches in $\mathbf{Z}_1$ have relatively high similarity and are very suitable for simultaneous sparse representation. Thus, simultaneous sparse representation is adopted in the first stage.

Nevertheless, $\hat{x}_1$ may still suffer from the common problem of artifact generation due to the intrinsic problem of any transform-domain methods, even if we are using a redundant learned dictionary. The second stage of refined filtering aims to remove them. It should be noted that we can also use sparse representation with a different kind of dictionary to remove the artifacts. However, the time consumption of sparse representation is very high and we need a more efficient technique to handle such task. With this respect, wavelet transform works effectively on each row of $\mathbf{Z}_2$ which is a smooth sequence after patch ordering. We also apply it to each column of $\mathbf{Z}_2$ to make the coefficients in the transform domain more sparse [44]. Thus, 2-D wavelet hard-thresholding is used in this stage. It should be noted that although the column is a lexicographic version of the patches which may not be smooth, with a suitable (generally low) threshold it will effectively work on the artifacts but rarely alter the original signal. Moreover, it runs much faster than sparse representation.

B. Parameter Selection

In the coarse filtering stage, 8×8 patches can ensure the accuracy of patch ordering. Thus, $n_1 = 64$. We set $SL_1^{(p)} = 2$ because it reduces the computation cost of SSC at only small cost of filtering performance. In Algorithm 1, we set $C = 17$. Note that this is much smaller than that in [32], where $C = 61$ and $C = 361$ are, respectively, used. However, such choices lead to unfavorable time complexity, making patch ordering unpractical to use for filtering large SAR images. In fact,

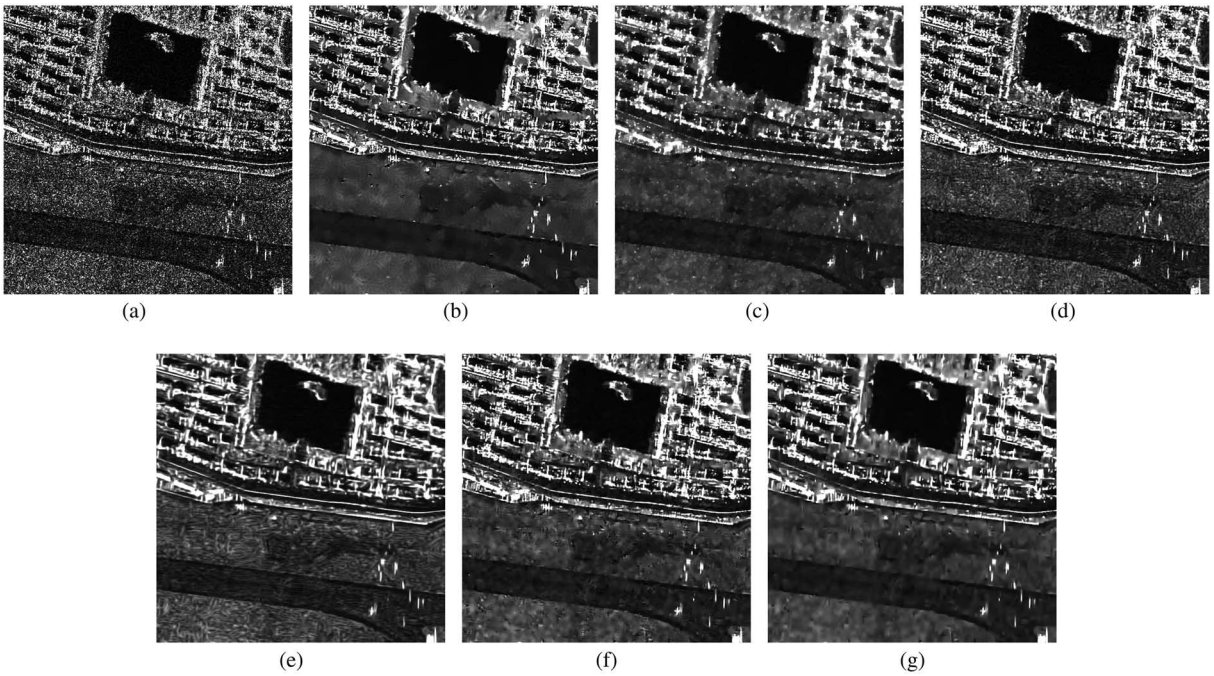

Fig. 9. Filtered images for Dalian. (a) Original image. (b) PPB. (c) MIDAL. (d) SAR-BM3D. (e) H-PO. (f) Coarse filtering. (g) Refined filtering.

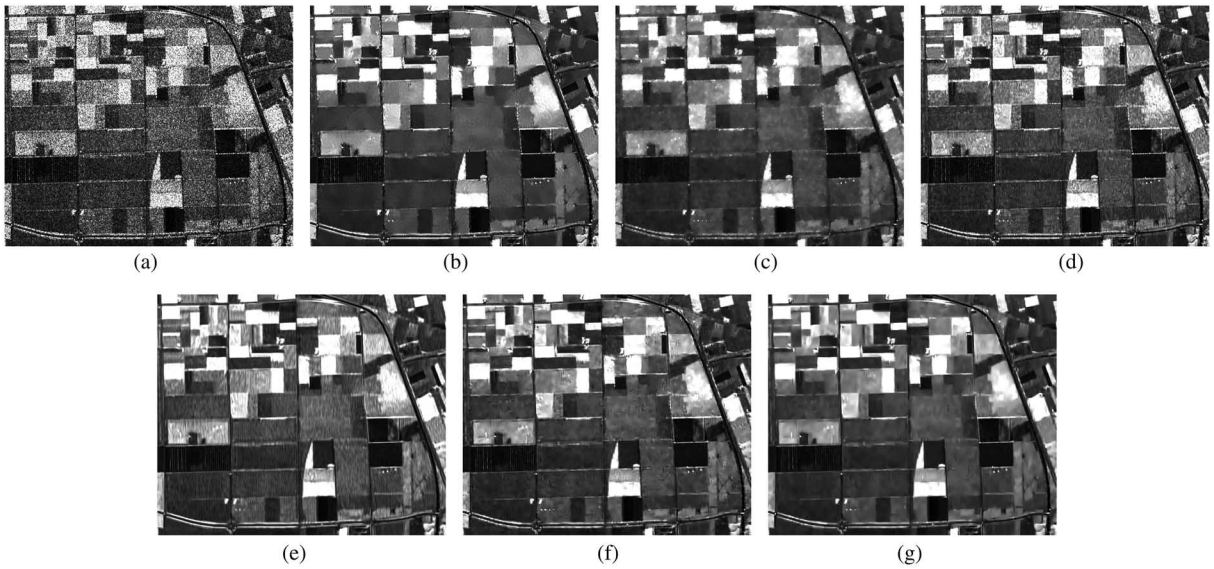

Fig. 10. Filtered images for Flevoland. (a) Original image. (b) PPB. (c) MIDAL. (d) SAR-BM3D. (e) H-PO. (f) Coarse filtering. (g) Refined filtering.

ordering of patches well finds its analogy to nonlocal filtering for search of similar patches [23], [25], [30]. Our choice of the searching window is in line with existing literature. The ordered patches $\mathbf{Z}_1$ is filtered by Algorithm 3, with the parameters $N^{(S)} = 8$, $N^{(t)} = 2000$, $N^{(i)} = 5$, and $k = 512$. Other parameters used for dictionary training are the same as in [37].

In the refined filtering stage, the ENL of $\hat{x}_1$ is much higher than I_B. Thus, $\hat{x}_1$ can be used for patch ordering again with a smaller patch size than that in the first stage. Here, n_2 is set to be 36. Since the time complexity of 2-D wavelet hard-thresholding is much smaller than SSC, $SL_2^{(p)} = 1$ is an appropriate choice.

TABLE IV
ENL OF FILTERED IMAGES

	Dalian		Flevoland	
	Region 1	Region 2	Region 1	Region 2
Noisy	1.00	1.00	2.99	2.98
PPB	**47.98**	**42.49**	207.10	**148.91**
MIDAL	27.17	24.22	151.05	122.42
SAR-BM3D	8.39	6.74	34.16	40.83
H-PO	12.04	12.20	44.49	39.26
Coarse filtering	26.47	19.72	117.98	92.84
Refined filtering	46.27	37.47	**244.94**	143.05

Best results are emphasized in boldface.

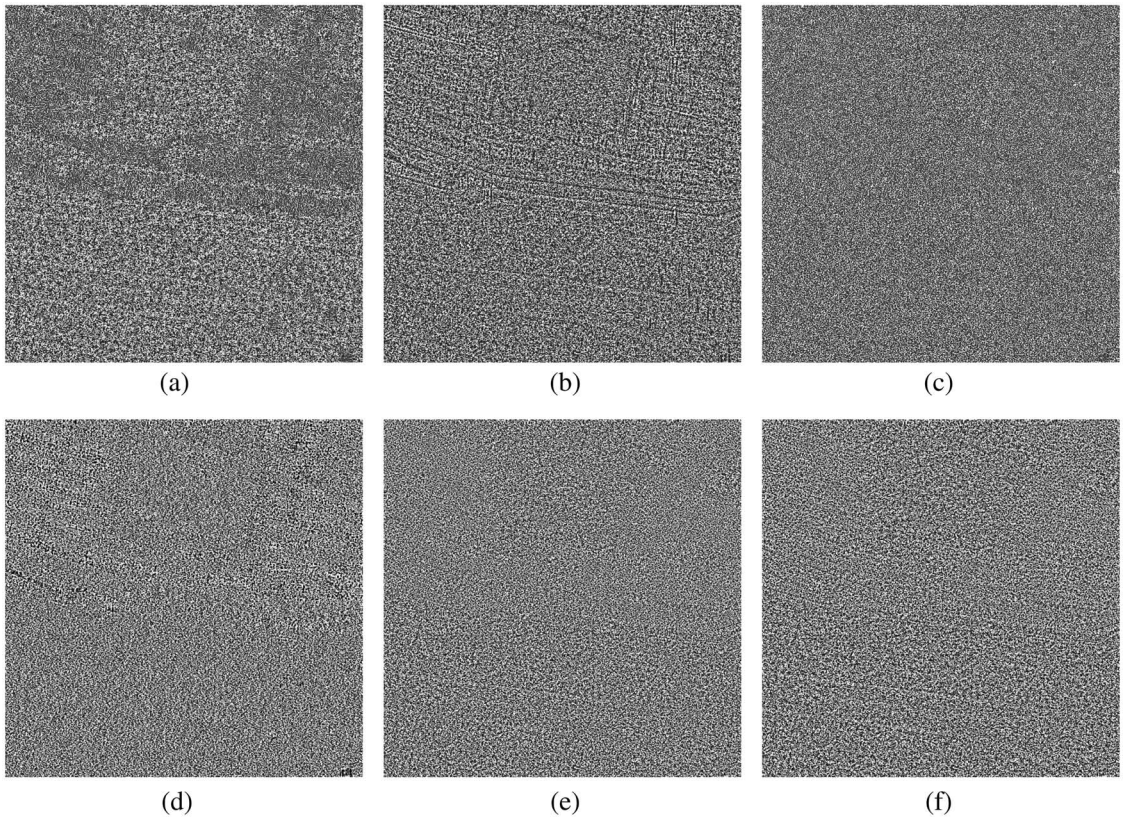

Fig. 11. Ratio image r for Dalian. (a) PPB. (b) MIDAL. (c) SAR-BM3D. (d) H-PO. (e) Coarse filtering. (f) Refined filtering.

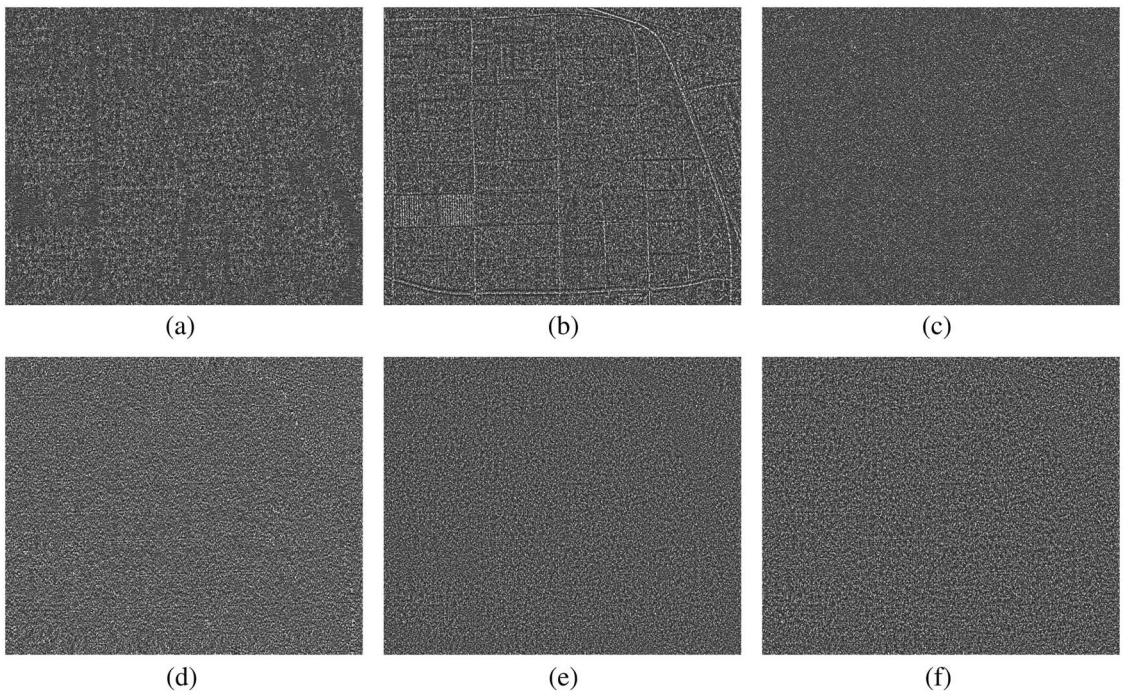

Fig. 12. Ratio image r for Flevoland. (a) PPB. (b) MIDAL. (c) SAR-BM3D. (d) H-PO. (e) Coarse filtering. (f) Refined filtering.

In this study, 2-D Haar wavelet transform with a four-level decomposition is adopted and λ is set to be $0.95\sqrt{\psi^{(1)}(L)}$.

The influences of some parameters will be discussed in Section V with experimental results.

V. Experimental Results

In this section, we use both simulated images and real SAR images to test the filtering performance of the proposed method. Simulated images are generated in the same way

as suggested in [23]. Two widely used 256×256 images, Peppers and Cameraman (see Fig. 5) are tested. For each optical image, we have simulated five images with $L = 1$, 2, 4, 8, and 16. In addition, two real SAR images (see Fig. 6) acquired from different SAR systems are used to further validate the effectiveness of the proposed method. They are, respectively, a 1-look TerraSAR-X image taken over Dalian in China, and a 4-look AIRSAR image taken over Flevoland in Netherlands.

The proposed method is compared with three state-of-the-art despeckling methods, PPB [27], MIDAL [7], and SAR-BM3D [23]. Moreover, we compare the proposed method with the homomorphic version of the original patch ordering method (H-PO) [32]. The coarse filtering results are also presented to verify the effectiveness of the refined filtering stage. The free parameters used in the proposed method are listed in Table I. The implementation code of the proposed method is available at [49]. For other methods, the free parameters are the same as in the reference papers. In Fig. 6, the pixels in the white box are used for ENL estimation which is realized by (3). The ENL estimation results for the test SAR images are 1.00 and 2.99, respectively. The estimated ENL is used as an input parameter in PPB, MIDAL, SAR-BM3D, H-PO, and the proposed method.

A. Results With Simulated Images

In this section, the filtering performance is evaluated by the peak signal-to-noise ratio (PSNR) and structural similarity (SSIM) index [46]. The PSNR and SSIM results for Peppers and Cameraman are shown in Tables II and III, respectively. The best results are emphasized in boldface. As suggested in [23], the results in Tables II and III are also obtained by averaging ten independent realizations of the noise process. One can see that the proposed method performs similar to SAR-BM3D and much better than the other methods.

With the increase in L, the filtering performance of the proposed method becomes better. The main reason of this behavior is that the learned dictionary which plays an important role in the proposed method becomes more and more suitable for SSC in Step 1 as L increases. Fig. 7(a) and (b) shows the learned dictionaries for Peppers with $L = 1$ and $L = 4$, respectively. When $L = 1$, the learned dictionary has a lot of meaningless patches which 7 are not helpful for sparse representation. When $L = 4$, the learned dictionary is much more suitable for SSC.

Filtered images for Peppers contaminated by 4-look speckle are shown in Fig. 8. It is found that PPB generates artifacts around the edges of the peppers and MIDAL introduces pointwise artifacts. On the other hand, SAR-BM3D, H-PO, and the proposed method have good speckle reduction ability and detail preserving ability, and produce fewer artifacts.

In Tables II and III, we find that the refined filtering stage achieves a PSNR gain of 0.5–1.5 dB, and a SSIM gain of 0.01–0.11. In Fig. 8, we can also find that the refined filtering stage removes most of the artifacts in the coarse filtering result. Thus the refined filtering stage is very effective.

In general, the proposed method achieves state-of-the-art despeckling performance for simulated images. The simulated speckle is white, whereas the speckle in real SAR images is correlated. Thus, we will focus on real SAR image despeckling in Section V-B.

TABLE V
MEAN VALUE AND ENL OF RATIO IMAGES. MEASURED ENL RESULTS ON ORIGINAL IMAGES ARE 1.00 FOR DALIAN AND 2.99 FOR FLEVOLAND, RESPECTIVELY

	Dalian		Flevoland	
	$E[r]$	ENL_r	$E[r]$	ENL_r
PPB	0.93	1.26	0.97	3.96
MIDAL	**1.00**	1.47	**1.00**	3.43
SAR-BM3D	0.90	1.89	0.95	5.32
H-PO	0.92	0.59	0.89	3.13
Coarse filtering	0.92	1.22	0.97	3.44
Refined filtering	0.97	**1.03**	0.99	**2.97**

Best results are emphasized in boldface.

B. Results With Real SAR Images

Filtered images for Dalian and Flevoland are shown in Figs. 9 and 10, respectively. We can find that MIDAL still introduces a number of pointwise artifacts in both flat regions and urban regions. PPB, SAR-BM3D, H-PO, and the proposed method have strong detail preserving ability in urban areas. However, the speckle reduction abilities of SAR-BM3D and H-PO are much more conservative than that in the simulated case. This is because the speckle in real SAR images are usually correlated, whereas SAR-BM3D and H-PO are developed under the hypothesis of uncorrelated speckle. Thus, for real SAR images, the proposed method and PPB achieve very good results.

Additionally, we use the ENL [4], [47] to evaluate the filtering results with real SAR images. The ENL indicates the speckle reduction ability in homogeneous regions and larger ENL corresponds to stronger speckle reduction ability. Table IV reports the ENL of filtered images using different despeckling methods. The best results are shown in boldface. For each image, we select two homogeneous regions (see Fig. 6) to calculate the ENL. From the ENL results, we can find that the proposed method and PPB have much stronger speckle reduction ability in homogeneous areas than MIDAL, SAR-BM3D, and H-PO.

Another commonly used indicator for SAR image despeckling is the ratio image [3], [4], [48] which represents the noise removed by SAR image despeckling. The ratio image is defined as the pointwise ratio between the original image I and filtered image $\hat{x}$

$$r = \frac{I}{\hat{x}}. \tag{22}$$

The best result corresponds to the ratio image r which is the closest to the actual speckle v. From the view of visual effect, the ratio image acquired by a good filter should be a pure random noise process. On the contrary, the ratio image obtained by an inferior filter contains structural information, especially

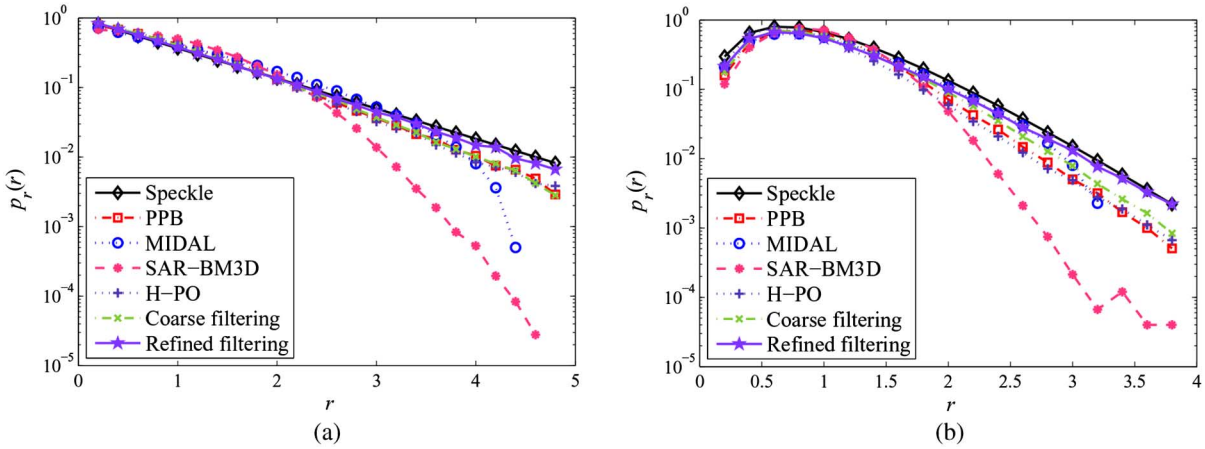

Fig. 13. PDF of r and the pdf of the actual speckle is used as a reference. "◊": the actual speckle; "□": PPB; "○": MIDAL; "•": SAR-BM3D; "+": H-PO; "×": Coarse filtering; "⋆": Refined filtering. (a) Dalian. (b) Flevoland.

at urban areas and edges. The ratio images for Dalian and Flevoland are given in Figs. 11 and 12, respectively. In Fig. 11, the SAR-BM3D ratio image has no obvious structural information, the ratio images acquired by the proposed method and H-PO have few edges, the MIDAL ratio image has much more edges and the PPB ratio also contains obvious structural information of both urban areas and edges. Similar phenomenon can also be observed in Fig. 12. From this point of view, SAR-BM3D, H-PO, and the proposed method perform much better than the other methods.

Moreover, we also analyze the ratio image with the following quantitative indicators: the mean of r, the ENL of r, and the probability density function (pdf) of r. The mean and ENL of r are often used to indicate the bias and speckle power suppression [4], [22], respectively. The pdf of r can be used to evaluate the similarity of r and v. Here we use the regions where the speckle is fully developed to calculate these indicators. In general, the speckle in flat areas such as road, grass and short vegetation is well developed. Thus in Fig. 6(a), the pixels in the red box are selected to analyze the ratio image. Fig. 6(b) is acquired over the farmlands in Flevoland. Thus, the whole image can be used to calculate the mean, ENL, and pdf of r. In Table V, we report the mean value and ENL of ratio images. From the results of $E[r]$, it can be observed that MIDAL has the smallest bias and the proposed method is the second best. From the results of ENL_r, we can conclude that the speckle power suppression of the proposed method is the best since the ENL of the ratio image acquired by the proposed method is the closest to the ENL estimated on the original image. In Fig. 13, we present the pdf of r for Dalian and Flevoland with logarithmic scale for the y-axis. The pdf of v is used as a reference. Particularly, the pdf of v for Dalian is exponential distribution (single-look speckle). Thus, it appears as a straight line in Fig. 13(a). For Flevoland, v follows the Gamma distribution, so the tailing part of the pdf seems like a straight line in Fig. 13(b). One can easily see that the pdf of r obtained by the proposed method is the closest to the pdf of v.

Combining the results of the mean, ENL, PDF, and visual effect of r, we can conclude that the ratio image achieved by the proposed method is the closest to the actual speckle. On the whole, the proposed method achieves the best results with real SAR images.

TABLE VI
COMPUTING TIME OF EACH STEP FOR DALIAN

	Procedure	Computing time
Step 1	Patch ordering	1.10 s
	SSC	12.55 s
Step 2	Patch ordering	1.87 s
	Wavelet hard-thresholding	8.43 s
Total		23.95 s

TABLE VII
PSNR (DB) AND SSIM RESULTS FOR PEPPERS WITH DIFFERENT SLIDING STEPS. $L = 4$

Parameters	PSNR	SSIM
$SL_1^{(p)} = 2$, $SL_2^{(p)} = 1$	28.87	0.846
$SL_1^{(p)} = 1$, $SL_2^{(p)} = 1$	28.89	0.843
$SL_1^{(p)} = 2$, $SL_2^{(p)} = 2$	28.37	0.833

In Tables IV and V, and Fig. 13, we can easily find that the refined filtering stage improves the filtering performance effectively since the refined filtering results are much better than the coarse filtering results. In Figs. 9 and 10, it is obvious that the refined filtering stage removes most of the artifacts in the coarse filtering result. Thus, we can conclude that the refined filtering stage is very important in the proposed method.

C. Time Consumption

The computation complexity of the proposed method is acceptable with a rational selection of parameters. Written in C source MEX-file and run by MATLAB, the proposed method is much faster than PPB and SAR-BM3D. Processing a 600×600 SAR image with the proposed method typically takes around 25 s, using a common PC of Intel Core i5 processor with 2.80-GHz main frequency and 8.00-GB main memory.

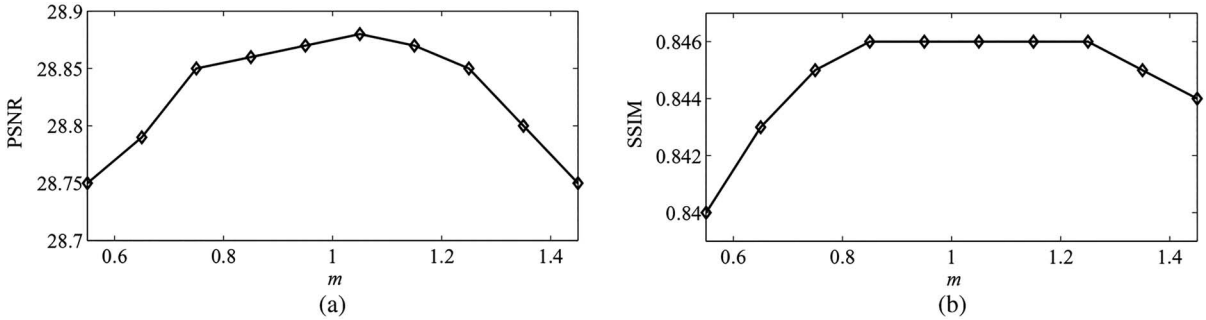

Fig. 14. PSNR (dB) and SSIM results for Peppers with different wavelet thresholds. $L = 4$. (a) PSNR. (b) SSIM.

Table VI gives the computing time of each step for Dalian (600×600). We can find that the simplified patch ordering algorithm for SAR images works very fast since the computing time of patch ordering only takes 12% of the total time. Denoising via SSC is a time-consuming process. If $SL_1^{(p)} = 1$, it takes around 50 s to filter the ordered patches of Dalian using SSC. Thus, it can greatly reduce the computation cost of SSC when $SL_1^{(p)} = 2$. In Section V-D, we will show that the cost of filtering performance is very small when we set $SL_1^{(p)} = 2$. Compared with SSC, the computing time of wavelet hard-thresholding is acceptable since it only takes around 8 s when $SL_2^{(p)} = 1$.

D. Discussion on Several Parameters

In this section, we mainly discuss the influences of three parameters, $SL_1^{(p)}$, $SL_2^{(p)}$, and λ. Table VII and Fig. 14 report the PSNR and SSIM results for Peppers contaminated by 4-look speckle with different sliding steps and wavelet thresholds, respectively. Other free parameters are the same as in Table I.

In Section V-C, we have showed that the rational selection of $SL_1^{(p)}$ can greatly reduce the computing time of SSC. In Table VII, we can see that the loss of PSNR is only 0.02 dB when $SL_1^{(p)} = 2$. On the contrary, the SSIM result becomes better when $SL_1^{(p)} = 2$. Thus, it is reasonable to set $SL_1^{(p)}$ to be 2. If $SL_2^{(p)} = 2$, the losses of PSNR and SSIM are very serious. Thus, $SL_2^{(p)}$ is set to be 1 in this study.

Let $m = \lambda/\sqrt{\psi^{(1)}(L)}$. In Fig. 14, we find that the rational selection of m can significantly improve the filtering performance. The PSNR and SSIM results are relatively good when $m \in [0.85,\ 1.15]$. Here, we set $m = 0.95$.

VI. Conclusion

In this paper, a novel SAR image despeckling method has been proposed. The homomorphic transformation was first applied and speckle filtering was implemented in the logarithmic domain. Specifically, the patch ordering method originally developed for additive white Gaussian noise was adapted to SAR images. Then, a two-stage filtering strategy was proposed. In the coarse filtering stage, the ordered patches of the logarithmic SAR image were filtered by learned SSC. In the refined filtering stage, the ordered patches of the coarse filtering result were further filtered by 2-D wavelet hard-thresholding. The final result was reconstructed from the refined filtering result by inverse permutation, subimage averaging, and exponential transformation.

We have used both simulated and real SAR images for validation of the proposed method. The results show, for simulated images, that the proposed method compares similarly to SAR-BM3D and achieves state-of-the-art performance in terms of PSNR and SSIM. For real SAR images, we used the ENL and ratio image to evaluate the filtering performance. The proposed method has very strong speckle reduction ability and the corresponding ratio image is the closest to the actual speckle. In addition, the computational time of the proposed method is also found acceptable for practical applications of SAR image processing.

Future work will focus on the following three aspects. First, the proposed method can be improved especially in 1-look case by improving the efficiency of dictionary learning which is also a challenging problem in sparse representation. Second, fast algorithm of the proposed method should be developed. Third, the proposed method will be extended to polarimetric SAR despeckling which is also a hot topic in SAR image processing.

Acknowledgment

The authors would like to thank Dr. C. Deledalle for providing PPB code and Prof. L. Verdoliva for her helpful comments and providing SAR-BM3D code. The authors would also like to thank the reviewers for their constructive comments.

References

[1] R. Touzi, A. Lopes, and P. Bousquet, "A statistical and geometrical edge detector for SAR images," *IEEE Trans. Geosci. Remote Sens.*, vol. 26, no. 6, pp. 764–773, Nov. 1988.

[2] J. S. Lee, M. R. Grunes, and G. De Grandi, "Polarimetric SAR speckle filtering and its impact on terrain classification," *IEEE Trans. Geosci. Remote Sens.*, vol. 37, no. 5, pp. 2363–2373, Sep. 1999.

[3] C. Oliver and S. Quegan, *Understanding Synthetic Aperture Radar Images With CDROM*, 2nd ed. Raleigh, NC, USA: SciTech, 2004.

[4] F. Argenti, A. Lapini, T. Bianchi, and L. Alparone, "A tutorial on speckle reduction in synthetic aperture radar images," *IEEE Geosci. Remote Sens. Mag.*, vol. 1, no. 3, pp. 6–35, Sep. 2013.

[5] H. Guo *et al.*, "Wavelet based speckle reduction with application to SAR based ATD/R," in *Proc. IEEE Int. Conf. Image Process.*, 1994, vol. 1, pp. 75–79.

[6] S. Solbø and T. Eltoft, "Homomorphic wavelet-based statistical despeckling of SAR images," *IEEE Trans. Geosci. Remote Sens.*, vol. 42, no. 4, pp. 711–721, Apr. 2004.
[7] J. M. Bioucas-Dias and M. A. T. Figueiredo, "Multiplicative noise removal using variable splitting and constrained optimization," *IEEE Trans. Image Process.*, vol. 19, no. 7, pp. 1720–1730, Jul. 2010.
[8] S. Foucher, "SAR image filtering via learned dictionaries and sparse representations," in *Proc. IEEE Int. Geosci. Remote Sens. Symp.*, 2008, vol. 1, pp. 229–232.
[9] J. Jiang, L. Jiang, and N. Sang, "Non-local sparse models for SAR image despeckling," in *Proc. IEEE Int. Conf. Comput. Vis. Remote Sens.*, 2012 pp. 230–236.
[10] M. Yang and G. Zhang, "SAR image despeckling using overcomplete dictionary," *Electron. Lett.*, vol. 48, no. 10, pp. 596–597, May 2012.
[11] Y. Huang, L. Moisan, M. K. Ng, and T. Zeng, "Multiplicative noise removal via a learned dictionary," *IEEE Trans. Image Process.*, vol. 21, no. 11, pp. 4534–4543, Nov. 2012.
[12] Y. Hao, X. Feng, and J. Xu, "Multiplicative noise removal via sparse and redundant representations over learned dictionaries and total variation," *Signal Process.*, vol. 92, no. 6, pp. 1536–1549, Jun. 2012.
[13] H. Xie, L. E. Pierce, and F. T. Ulaby, "Statistical properties of logarithmically transformed speckle," *IEEE Trans. Geosci. Remote Sens.*, vol. 40, no. 3, pp. 721–727, Mar. 2002.
[14] J. S. Lee, "Digital image enhancement and noise filtering by use of local statistics," *IEEE Trans. Pattern Anal. Mach. Intell.*, vol. PAMI-2, no. 2, pp. 165–168, Mar. 1980.
[15] V. S. Frost, J. A. Stiles, K. S. Shanmugan, and J. C. Holtzman, "A model for radar images and its application to adaptive digital filtering of multiplicative noise," *IEEE Trans. Pattern Anal. Mach. Intell.*, vol. PAMI-4, no. 2, pp. 157–166, Mar. 1982.
[16] D. T. Kuan, A. A. Sawchuk, T. C. Strand, and P. Chavel, "Adaptive noise smoothing filter for images with signal-dependent noise," *IEEE Trans. Pattern Anal. Mach. Intell.*, vol. PAMI-7, no. 2, pp. 165–177, Mar. 1985.
[17] A. Lopes, R. Touzi, and E. Nezry, "Adaptive speckle filters and scene heterogeneity," *IEEE Trans. Geosci. Remote Sens.*, vol. 28, no. 6, pp. 992–1000, Nov. 1990.
[18] D. T. Kuan, A. A. Sawchuk, T. C. Strand, and P. Chavel, "Adaptive restoration of images with speckle," *IEEE Trans. Acoust. Speech Signal Process.*, vol. ASSP-35, no. 3, pp. 373–383, Mar. 1987.
[19] A. Lopes, E. Nezry, R. Touzi, and H. Laur, "Maximum a posteriori speckle filtering and first order texture models in SAR images," in *Proc. IEEE Int. Geosci. Remote Sens. Symp.*, 1990, vol. 3, pp. 2409–2412.
[20] H. Xie, L. Pierce, and F. Ulaby, "Despeckling SAR images using a low complexity wavelet denoising process," in *Proc. IEEE Int. Geosci. Remote Sens. Symp.*, 2002, vol. 1, pp. 321–324.
[21] F. Argenti, T. Bianchi, and A. Alparone, "Multiresolution MAP despeckling of SAR images based on locally adaptive generalized Gaussian pdf modeling," *IEEE Trans. Image Process.*, vol. 15, no. 11, pp. 3385–3399, Nov. 2006.
[22] F. Argenti, T. Bianchi, and A. Alparone, "Segmentation-based MAP despeckling of SAR images in the undecimated wavelet domain," *IEEE Trans. Geosci. Remote Sens.*, vol. 46, no. 9, pp. 2728–2742, Sep. 2008.
[23] S. Parrilli, M. Poderico, C.V. Angelino, and L. Verdoliva, "A nonlocal SAR image denoising algorithm based on LLMMSE wavelet shrinkage," *IEEE Trans. Geosci. Remote Sens.*, vol. 50, no. 2, pp. 606–616, Feb. 2012.
[24] B. Hou, X. Zhang, X. Bu, and H. Feng, "SAR image despeckling based on nonsubsampled shearlet transform," *IEEE J. Sel. Topics Appl. Earth Observ. Remote Sens.*, vol. 5, no. 3, pp. 809–823, Jun. 2012.
[25] A. Buades, B. Coll, and J. M. Morel, "A review of image denoising algorithms, with a new one," *Multiscale Model. Simul.*, vol. 4, no. 2, pp. 490–530, Jul. 2005.
[26] P. Coupé, P. Hellier, C. Kervrann, and C. Barillot, "Bayesian non local means-based speckle filtering," in *Proc. IEEE Int. Symp. Biomed. Imag.*, 2008, pp. 1291–1294.
[27] C. Deledalle, L. Denis, and F. Tupin, "Iterative weighted maximum likelihood denoising with probabilistic patch-based weights," *IEEE Trans. Image Process.*, vol. 18, no. 12, pp. 2661–2672, Dec. 2009.
[28] C. Jojy, M. S. Nair, G. R. K. S. Subrahmanyam, and R. Riji, "Discontinuity adaptive non-local means with importance sampling unscented Kalman filter for de-speckling SAR images," *IEEE J. Sel. Topics Appl. Earth Observ. Remote Sens.*, vol. 6, no. 4, pp. 1964–1970, Aug. 2013.
[29] J. Chen, Y. Chen, W. An, Y. Cui, and J. Yang, "Nonlocal filtering for polarimetric SAR data: A pretest approach," *IEEE Trans. Geosci. Remote Sens.*, vol. 49, no. 5, pp. 1744–1754, May 2011.
[30] K. Dabov, A. Foi, V. Katkovnik, and K. Egiazarian, "Image denoising by sparse 3D transform-domain collaborative filtering," *IEEE Trans. Image Process.*, vol. 16, no. 8, pp. 2080–2095, Aug. 2007.
[31] D. Cozzolino, S. Parrilli, G. Scarpa, G. Poggi, and L. Verdoliva, "Fast adaptive nonlocal SAR despeckling", *IEEE Geosci. Remote Sens. Lett.*, vol. 11, no. 2, pp. 524–528, Feb. 2014.
[32] I. Ram, M. Elad, and I. Cohen, "Image processing using smooth ordering of its patches," *IEEE Trans. Image Process.*, vol. 22, no. 7, pp. 2764–2774, Jul. 2013.
[33] I. Ram, M. Elad, and I. Cohen, "Image denoising using NL-Means via smooth patch ordering," *IEEE Int. Conf. Acoust. Speech Signal Process (ICASSP)*, pp. 1350–1354, May 2013.
[34] M. Elad and M. Aharon, "Image denoising via sparse and redundant representations over learned dictionaries," *IEEE Trans. Image Process.*, vol. 15, no. 12, pp. 3736–3745, Dec. 2006.
[35] J. Mairal, M. Elad, and G. Sapiro, "Sparse representation for color image restoration," *IEEE Trans. Image Process.*, vol. 17, no. 1, pp. 53–69, Jan. 2008.
[36] J. Mairal, F. Bach, J. Ponce, G. Sapiro, and A. Zisserman, "Non-local sparse models for image restoration," in *Proc. IEEE Int. Conf. Comput. Vis.*, 2009, pp. 2272–2279.
[37] M. Aharon, M. Elad, and A. M. Bruckstein," The K-SVD: An algorithm for designing of overcomplete dictionaries for sparse representations," *IEEE Trans. Signal Process.*, vol. 54, no. 11, pp. 4311–4322, Nov. 2006.
[38] Y. Cui, G. Zhou, J. Yang, and Y. Yamaguchi, "Unsupervised estimation of the equivalent number of looks in SAR images," *IEEE Geosci. Remote Sens. Lett.*, vol. 8, pp. 710–714, Jul. 2011.
[39] B. Xu, Y. Cui. G. Zhou, B. You, J. Yang, and J. Song, "Unsupervised speckle level estimation of SAR images using texture analysis and AR model," *IEICE Trans. Commun.*, vol. E97-B, no. 3, pp. 691–698, Mar. 2014.
[40] R. R. Coifman and D. L. Donoho, "Translation-invariant de-noising," in *Wavelets and Statistics*. New York, NY, USA: Springer, 1995, pp. 125–150.
[41] J. A. Tropp, "Greed is good: Algorithmic results for sparse approximation," *IEEE Trans. Inf. Theory*, vol. 50, no. 10, pp. 2231–2242, Oct. 2004.
[42] J. A. Tropp, "Algorithms for simultaneous sparse approximation," *Signal Process.*, vol. 86, pp. 572–602, 2006.
[43] R. Rubinstein, A. M. Bruckstein, and M. Elad, "Dictionaries for sparse representation modeling," *Proc. IEEE*, vol. 98, no. 6, pp. 1045–1057, Jun. 2010.
[44] I. Ram, M. Elad, and I. Cohen, "Generalized tree-based wavelet transform," *IEEE Trans. Signal Process.*, vol. 59, no. 9, pp. 4199–4209, Sep. 2011.
[45] V. Katkovnik, A. Foi, K. Egiazarian, and J. Astola, "From local kernel to nonlocal multiple-model image denoising," *Int. J. Comput. Vis.*, vol. 86, pp. 1–32, 2010.
[46] Z. Wang, A. C. Bovik, H. R. Sheikh, and E. P. Simoncelli, "Image quality assessment: From error visibility to structural similarity," *IEEE Trans. Image Process.*, vol. 13, no. 4, pp. 600–612, Apr. 2004.
[47] S. G. Dellepiane and E. Angiati, "Quality assessment of despeckled SAR images," *IEEE J. Sel. Top. Appl. Earth Observ. Remote Sens.*, vol. 7, no. 2, pp. 691–707, Feb. 2014.
[48] R. Touzi, "A review of speckle filtering in the context of estimation theory," *IEEE Trans. Geosci. Remote Sens.*, vol. 40, no. 11, pp. 2392–2404, Nov. 2002.
[49] [Online]. Available: http://oa.ee.tsinghua.edu.cn/%7eyangjian/xubin/code/SAR-POTDF-v0.1.zip

Bin Xu received the B.S. degree in information and communication engineering from Tsinghua University, Beijing, China, in 2011, where he is currently pursuing the Ph.D. degree in information and communication engineering at the Department of Electronic Engineering.

His research interests include SAR image processing and polarimetric SAR image processing.

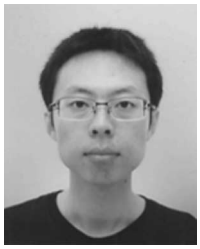

Yi Cui (S'09–M'11) received the B.S. degree (Hons.) in electronic information science and technology from Jilin University, Changchun, China, in 2006, and the Ph.D. degree in information and communication engineering from Tsinghua University, Beijing, China, in 2011.

From 2011 to 2014, he was with Niigata University, Niigata, Japan. He is now with the Global Institute for Collaborative Research and Education, Hokkaido University, Sapporo, Japan.

Dr. Cui is an Associate Editor of the IEEE JOURNAL OF SELECTED TOPICS IN APPLIED EARTH OBSERVATION AND REMOTE SENSING. He has been recognized as the 2013 Best Reviewer of the IEEE TRANSACTIONS ON GEOSCIENCE AND REMOTE SENSING. He was the first-prize winner of the student paper competition at the 2010 Asia-Pacific Radio Science Conference (AP-RASC10), the recipient of the Best Paper Award of the 2012 International Symposium on Antennas and Propagation, and the recipient of the 2013 IEEE Geoscience and Remote Sensing Society Symposium Prize Paper Award.

Zenghui Li received the B.S. degree in electronic and engineering from Beihang University, Beijing, China, in 2005, and the M.S. degree in information and communication technology from the National University of Defense Technology, Changsha, China, in 2007. Currently, he is pursuing the Ph.D. degree in information and communication engineering at the Department of Electronic Engineering, Tsinghua University, Beijing, China.

His research interests include polarimetric SAR image processing.

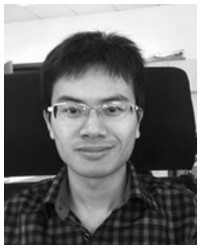

Bin Zuo received the B.S. degree in information and communication engineering from Tsinghua University, Beijing, China, in 2013, where he is currently pursuing the Ph.D. degree in information and communication engineering at the Department of Electronic Engineering.

His research interests include polarimetric SAR image processing.

Jian Yang (M'98–SM'02) received the B.S. and M.S. degrees from the Northwestern Polytechnical University, Xian, China, in 1985 and 1990, respectively, and the Ph.D. degree from Niigata University, Niigata, Japan, in 1999.

In 1985, he was with the Department of Applied Mathematics, Northwestern Polytechnical University. From 1999 to 2000, he was an Assistant Professor with Niigata University. In April 2000, he was with the Department of Electronic Engineering, Tsinghua University, Beijing, China, where he is currently a Professor. His interests include radar polarimetry, remote sensing, mathematical modeling, optimization in engineering, and fuzzy theory.

Dr. Yang is an Associate Editor of the IEEE TRANSACTIONS ON GEOSCIENCE AND REMOTE SENSING, the Vice-Chairman of the IEEE AEROSPACE AND ELECTRONIC SYSTEMS in Beijing chapter, and the former Chairman of the Institute of Electronics, Information, and Communication Engineers, Beijing, China.

Jianshe Song received the B.S. degree in mathematics from Shanxi Normal University, Xi'an, China, in 1982, and the M.S. and Ph.D. degrees in mathematics from Xidian University, Xi'an, China, in 1989 and 2001, respectively.

Currently, he is a Professor with Xi'an Research Institute of Hi-Technology, Xi'an, China. He has finished many projects and received more than 10 awards from Chinese government. He has authored/coauthered five books and more than 150 papers. His research interests include radar theory, signal processing, and optimization in engineering.